ESAIM: PROCEEDINGS AND SURVEYS, 2017, Vol. 57, p. 23-36
Oana Silvia Serea & Walter Briec Editors

PREDICTABILITY OF MARINE POPULATION TRAJECTORIES–THE EFFECT OF DELAYS AND RESOURCE AVAILABILITY *

Anna S. J. Frank[1]

Abstract. This paper studies the dynamics and stability of a stage-structured (immature/mature) population. The emphasis is on how resource available to the immature stage indirectly regulates the dynamics of the mature stage, where the resource is defined by a Holling-II function. We present the results from numerical experiments, where inference about stability and predictability of the system dynamics is based on the theory of Lyapunov exponents.

Résumé. Cet article étudie la dynamique et la stabilité d'une population structurée en stades (immature/mature). L'accent est mis sur la faǫn dont la ressource disponible au stade immature contrôle indirectement la dynamique du stade mature, la ressource étant définie par une fonction de type Holling-II. Nous présentons les résultats d'expériences numériques, dans lesquelles l'inférence sur la stabilité et la prévisibilité de la dynamique du système est basée sur la théorie des exposants de Lyapunov.

Introduction

In the literature, resource availability is considered as limiting factor of population growth [48]. Ecologists have observed this phenomenon, explicitly for single-species, where population dynamics tend to fluctuate, cycle or exhibit behaviors that depend on resource [49, 50, 52]. Furthermore, examples of existing ecological models with delays are, for instance, chemostat models, which exemplify marine ecosystems [53–58].

In [51], it is shown that two disjoint species may react differently to their changing food environments. How changing resource can affect the dynamics and stability of a marine population is shown in [29]. The latter article analyzes a two-stage structured (mature/immature) population model with a delay term in the conversion of resource into biomass. The significance of different functional representations of the resource was investigated, and it was analyzed how varying functional parametrizations lead to different types of dynamic forcing at the immature population stage.

Motivated by [29], the aim of this paper is to analyze the combined effect of resource availability and delays on a dynamical systems. Depending on a changing resource availability and delays, we analyze sensitivity to initial conditions and the system predictability . The forecast horizon and predictability of the time series will be based on maximum Lyapunov exponents (MLEs).

General system dynamics for $x(t) \in \mathbb{R}^n$ can be described by the autonomous ordinary differential equation (ODE) system (1), where f is a functional operator [15]. It is possible to obtain analytical results about the system stability, sensitivity to initial conditions, and predictability, and there is an abundance literature on

* *I am grateful to Prof. Dr. Christina Kuttler (TUM) and Dr. Sam Subbey (IMR) for helpful feedback and comments.*

[1] Now at: Department of Pharmacy, Faculty of Mat. and Nat. Sciences, Univ. of Oslo, e-mail: a.s.j.frank@farmasi.uio.no

these issues [10–14].

$$\dot{x}(t) = f(t, x(t)) \tag{1}$$

A variant of system (1) is given by (2), which involves, in addition, a previous solution $x(t-\tau)$ of $x(t)$ at $0 < \tau \leq T,\ T \in \mathbb{R}$, τ-time-steps in the past and given initial conditions $\phi : [-\tau, 0] \to \mathbb{R}^n$, with $x(0) = \phi(0)$ [15, 16],

$$\dot{x}(t) = f(t, x(t), x(t-\tau)). \tag{2}$$

The parameter τ is called *delay*. System (2) can depend on several delays, see [16]. For this particular system, obtaining closed form solutions is challenging, and analytical tools are either unavailable or limited. Time series analysis offers a viable approach to obtaining information about the system dynamics. The approach involves applying time series analysis methodologies to a finite data set from the system defined by (2). This has the advantage of making inference on the system dynamics without knowing the exact mathematical model structure. A particular challenge to the time series application arises when the system dynamics is sensitive to initial conditions.

The Lyapunov exponents present a methodological approach for the study of such chaotic series [6, 17–19]. The exponents help in classifying system characteristics, and for time series prediction, see [19, 23–26]. For the system defined by (2), the Lyapunov exponents can be determined from the system time series [20] or by an approximation of the delay terms, see [21].

This manuscript applies the methodology of a time series approach, in order to analyze how the predictability and dynamical structure of a single-species population is influenced with respect to its resource availability and its delay-time, τ, in biomass growth.

1. Model and Methods and Materials

1.1. Model Description

Table 1. *Nomenclature*

$z(t) \in \mathbb{R}_+$	Resource biomass
$x(t) \in \mathbb{R}_+$	Biomass of immature population
$y(t) \in \mathbb{R}_+$	Biomass of mature population
$z^*,\ x^*,\ y^* \in \mathbb{R}_+$	Equilibrium values
$t \in \mathbb{R}$	Simulation time
$\tau_i \in \mathbb{R}, i \in \{1, 2\}$	Time delays
$f(z(t), \boldsymbol{\theta})$	Resource-growth-function
$\boldsymbol{\theta} \in \mathbb{R}$	Parameter-set
$a_x \in \mathbb{R}_+$	Resource uptake rate of the immature
$\mu \in (0, 1)$	Resource conversion rate into biomass
$d_x \in (0, 1), d_y \in (0, 1)$	Mortality of $x(t), y(t)$
$\delta \in (0, 1)$	Maturation rate

Throughout this work, we adopt the nomenclature in Tableau 1. The base-case model S_0 is given by (3):

$$S_0 \equiv \begin{cases} \dot{z}(t) &= f(z(t), \boldsymbol{\theta}) - a_x z(t) x(t), \\ \dot{x}(t) &= \mu a_x z(t-\tau_1) \cdot x(t-\tau_1) - d_x x(t) - \delta x(t), \\ \dot{y}(t) &= -d_y y(t) + \delta x(t-\tau_2), \end{cases} \tag{3}$$

with $\tau_2 \approx 0$ and $f(z(t), \boldsymbol{\theta}) : \mathbb{R}_+ \mapsto \mathbb{R}_+$ defined by (4),

$$f(z(t), \boldsymbol{\theta}) = \frac{az(t)}{b + z(t)}, \tag{4}$$

where $a = \alpha b$ with $a \in \mathbb{R}_+$, $b \in \mathbb{R}_+$ and $\alpha \in \mathbb{R}_+$. The resource-growth function $f(z(t), \boldsymbol{\theta})$ in equation (4) is known as the Holling-II function.

The parameter d_x and d_y are the death rates, respectively of the immature and the mature population, while δ is the rate at which a part of the immature stage transitions to the mature stage. The constant a_x represents the scale of food uptake at $(t - \tau_1)$, with τ_1 representing the delay in the feedback-cycle between ingestion and biomass growth. The parameter μ controls how much of the resource uptake is converted into biomass. Thus, the food induced biomass change $\dot{x}(t)$ at t, is regulated by the prior population biomass and the resource density. The mature population changes in its biomass $\dot{y}(t)$ due to maturation and natural mortality.

The fixed model parameters are summarized in Tableau 2 and represent synthetic values.

TABLE 2. *Fixed model parameters*

Parameter	a_x	μ	d_x	d_y	$\{h_1, h_2, h_3\}$	δ
Value	1.6	0.4	0.2	0.15	$\{2, 1, 0.5\}$	0.35

1.2. **Analysis of time series from the system** S_0

We use non-linear methods to analyze the time series. In this section, x_t is used for illustration. The analysis also applies to z_t, y_t.

However, we first need to establish that the time series is indeed non-linear, see [30]. Next, we determine the embedding dimension of the underlying dynamic, and ultimately the MLEs.

Non-linearity Test

Non-Gaussianity is indicative of non-linearity of a time series [30]. The approach for testing Gaussianity involves third order moments and surrogate data testing. The third order moment of a Gaussian time series is zero, see [31], while surrogate data tests are based on hypothesis testing, build on assumption of the statistical distribution of the observed time series.

Given the moment generating function $M(t_1, t_2, ..., t_n)$, the third order moment is given by the third derivative of the moment generating function at $t = 0$ [31].

In the applied non-linearity test, we calculate the third order moment and compare its expected value with the third order moment of the time series of the surrogate data, generated by the Amplitude Adjusted Fourier transform (AAFT) method.

Surrogate data test

The surrogate data test consists of a null hypothesis H_0 of a given data set, see [32,33]. The significance level of the test is given by α. The non-linearity test used in the following, considers the null H_0 and the alternative H_1 hypotheses defined by,

$$H_0 \equiv \{x_t \text{ is generated by linear Gaussian process}\},$$

$$H_1 \equiv \{x_t \text{ is not generated by linear Gaussian process}\}.$$

The surrogate data is generated using a method of Fourier Transform (FT) and phase randomization. The FT of a time series $x = (x_1, ..., x_N)$ with length N and zero mean, is given by [33],

$$F(\omega) = \frac{1}{\sqrt{2\pi N}} \sum_{t=1}^{N} e^{-i\omega t} x_t, -\pi \leq \omega \leq \pi. \tag{5}$$

The surrogate data $\tilde{x}_t$, with fixed Fourier amplitudes $|F(\omega_j)|$ and uniform distributed random numbers $\phi_{rand}(\omega_j) \in [0, 2\pi]$, is given by,

$$\tilde{x}_t = \sqrt{\frac{2\pi}{N}} \sum_{j=1}^{N} e^{i\omega_j t} |F(\omega_j)| e^{i\phi_{rand(\omega_j)}}. \tag{6}$$

The original data can be reconstructed by the inverse FT, see [33]. The FT surrogates $\tilde{x}_t$ are asymptotically uniform and normal distributed. Therefore, it can be easily established whether the surrogates do have the same distribution as the original data.

AAFT method

This method assumes, that the surrogate time series and the original time series are comparable on the basis of their higher-order moments. Hence, to test if the original data and the surrogate data are derived from the same distribution, one uses the Skewness and Kurtosis, i.e. third and fourth order moments of the original and surrogate time series.

Bootstrapping is used to compare the Skewness, i.e. measure of symmetry around the mean of the time series, of the original with the surrogate time series based on test statistics, see [31, 34, 35].

- If these third-order moments are equal for both series, we conclude that the original data is linear.

The bootstrapping method from [34], aims to find a third-order estimate in the region $0 \leq \xi_1 \leq \xi_2 \leq M$, with M as a truncation value ($1 \leq M \leq N$). The integers ξ_1 and ξ_2 define the serial indicates for the calculation of the third-order moments, i.e. $X_l, X_{l+\xi_1}, X_{l+\xi_2}$. And $\Delta^{\#} := \{(\xi_1, \xi_2) : 0 \leq \xi_1 \leq \xi_2 \leq M, \xi_1 + \xi_2 > 0\}$ defines the regions of the bootstrap series. The cardinality of the test is $T^{\#} := \frac{(M+1)(M+2)}{2} - 1$. For more details see [34].

The Embedding Parameters–τ and D_{E^*}

We lack essential information about the *true* dynamical system of the time series. The delay τ and the embedding dimension D_{E^*} characterize the underlying system dynamics, such that we are able to reconstruct the phase-space of the true dynamical system of the time series [36]. Determining the delay, τ, we apply the Average Mutual Information (AMI)-method, and for the embedding dimension, D_{E^*}, we calculate the False-Nearest Neighbors (FNN) from the time series. Given that AMI is based on probability densities, it detects the density of episodes, which resemble each other and therefore lie close together in the phase space [37, 38].

Definition 1.1. *(Average Mutual Information (AMI))*
Let $x_n, n \in [N], N \in \mathbb{N}$ be a data series and $x_{n+\tau}$ be delayed data points. Further, define $P(x_n)$ as frequency distribution of a single data point. The joint probability of two data points, x_n and $x_{n+\tau}$, is then given by $P(x_n, x_{n+\tau})$. In [38], the AMI with respect to time series delay τ, is specified via,

$$I(\tau) = -\sum_{i=1}^{N} P(x_n, x_{n+\tau}) ln \left(\frac{P(x_n, x_{n+\tau})}{P(x_n) \cdot P(x_{n+\tau})} \right). \tag{7}$$

The optimal τ is given by

$$\begin{cases} \underset{\tau}{\text{argmin}}\ I(\tau) \\ s.\ t. \quad \forall\ \tau^{'} < \tau :\ I(\tau) < I(\tau^{'}) \end{cases} \tag{8}$$

Numerically, the optimal delay is easy to find. One simply has to plot $I(\tau)$ against the τ-range, and choose the τ of the first minimum, see [37,38].

Given τ, we are able to construct d-dimensional *delay vectors* y defined by,

$$w \in \mathbb{R}^d,\ w = [x_n, x_{n+\tau}, ..., x_{n+(d-1)\tau}], \tag{9}$$

with $n = 1$, and $N' = N - (d-1)\tau$, see [24, 37, 38], which, all together, reconstruct an orbit. d is called the embedding dimension, see [24]. The concept of False Nearest Neighbors (FNN) helps detect the appropriate embedding dimension D_{E^*} in the following way:

Two nearby vectors w^1 and w^2 of the form (9), are referred to as FNNs if, given a certain threshold R, [38],

$$\frac{|x^1_{n+d\tau} - x^2_{n+d\tau}|_1}{||x^1_{n+d\tau} - x^2_{n+d\tau}||_2} \quad > \quad R, \tag{10}$$

where $||.||_\ell$ refers to the ℓ-norm.

Extending the embedding dimension d, step-by-step by 1, such that the number of neighbors drops, while the number of FNNs increases, yields the optimal embedding dimension D_{E^*}, [38].

Definition 1.2. *(Embedding D_{E^*})*
The embedding dimension $D_{E^*} = d + i,\ i \in \mathbb{N}$, when,

$$\frac{\#\textit{neighbors in dimension } d+i,}{\#\textit{neighbors in dimension } d} \to 0. \tag{11}$$

Plotting the quotient in equation (11) against $d + i$, $i \in \mathbb{N}$, we derive a monotone decreasing curve as i increases. The curve tends to zero for $i \to \infty$. Hence, D_{E^*} equals $d + i$ at the first local minimum.

Maximum Lyapunov exponent (MLE)

The MLE describes, how small errors $\delta_0 = |x_n - x_n^{'}|$ between recurrent points x_n, x'_n of a (time series) trajectory $\mathcal{X}_n$ will develop (exponentially) in its future error $\delta_l = |x_{n+l} - x'_{n+l}|$, $l \in \mathbb{N}$ samples ahead, see [24,28],

Definition 1.3. *(MLE)*
The MLE λ_1 is given by

$$|\delta_l| \quad \approx \quad \delta_0 e^{\lambda_1 l}. \tag{12}$$

A positive MLE indicates limited predictability, while a negative MLE promises unlimited prediction. The MLEs in this article are determined computationally, with either the algorithm of Kantz [40], Rosenstein [9] or Wolf [19].

Predictability and Forecast Horizon

For $\lambda_1 > 0$ the forecast time horizon (prediction time) T_p is finite, see [39]. However a $\lambda_1 < 0$ results in the forecast horizon $T_p = \infty$, see [39].

Given a delay vector $[x_{(m-1)\tau+1}, ..., x_N] \in \mathbb{R}^m$ the aim is to forecast a new measurement, Δn time steps in the future based on the last measurement x_N, given a threshold ϵ. Its value has to be chosen, such that all values within this threshold are candidates for good forecasts of x_N. Hence, we define the neighborhood $U_\epsilon(x_N)$ around x_N containing all points less than ϵ away from x_N.

For all the points in the neighborhood $U_\epsilon(x_N)$, we find the embedding vectors $x_n \in U_\epsilon(x_N)$ and predict their values, $x_{n+\Delta n}$.

The prediction $\hat{x}_{N+\Delta n}$ of x_N is then given by the average over all forecasts $x_{n+\Delta n}$, see [40],

$$\hat{x}_{N+\Delta n} = \frac{\sum_{x_n \in U_\epsilon(x_N)} x_{n+\Delta n}}{|U_\epsilon(x_N)|}. \tag{13}$$

The divergence in the neighboring points indicate how good the prediction $\hat{x}_{N+\Delta n}$ is, compared to the prediction of point $x_{N+\Delta n}$ in direction of the delay-coordinate. A small forecast error indicates that the predictions $\hat{x}_{N+\Delta n}$ and $x_{n+\Delta n}$ are close, and thus we can accept the prediction to be good.

The difference between $\hat{x}_{N+\Delta n}$ and the prediction of $x_{N+\Delta n}$ is calculated for each n time step ahead and defined as the *root mean squared (rms) forecast error*, Error $:= ||\hat{x}_{N+\Delta n} - x_{N+\Delta n}||_2$.

The concept is implemented computationally and used applied in the following experiments.

2. Numerical Experiments

We consider model S_0 from system (3) with the Holling-II function as resource-growth function. For the experiments, we aim to vary the Holling-II function to see the effect of a changing food-basis on the mature population for $\tau_1 = 0$ and $\tau_1 \neq 0$. We consider two situations conditioned on the parameters $\boldsymbol{\theta} = \{a, b\}$.

Table 3. *Scenarios of the numerical experiments*

Scenario	Condition	
	$\boldsymbol{\theta}$-condition	τ_1
1	$a = b$	0
2	$a = b$	1.2
3	$a < b$	0

The Scenarios for the numerical experiments are summarized in Tableau 3.

2.1. Experimental Scenarios

Scenario 2 is a sub-case of Scenario 1, as we increase only the delay value τ_1. Scenario 3 looks at the effect of changed resource-growth-parameters $\boldsymbol{\theta}$ on the dynamics for $\tau_1 = 0$.

The goal of the experiments is to detect the *critical* $\tau^* \in \mathbb{R}_+$, as well as to study the effect of τ_1 under different resource-growth-parameters $\boldsymbol{\theta}$. τ^* is *critical* in the sense that we expect a change of dynamics at τ^*, such that the dynamics for $\tau_1 < \tau^*$ are significantly different from the dynamics for $\tau^* < \tau_1$.

For each of the Scenarios, we follow the procedure described in Section 1.2, by checking for the time series non-linearity and by applying non-linear methods to determine MLE, and predictability of the system, see [41].

3. Results

We start with the presentation of the results, both from the non-linearity test and the model analysis. This is followed by a discussion and summary. The model time series and the reconstructed phase space dynamics of the mature series are presented.

3.1. Results

This section begins with the test for non-linearity on the mature time series and moves on to the model analysis for the different scenarios. For the sake of brevity we concentrate on the analysis results for the mature stage only.

The test-results from Tableau 4 show that all time series of model S_0 are non-linear.

The results from the model analysis are summarized in Tableau 5.

TABLE 4. *Non-linearity test*

Non-linearity test	Results		
Scenario	1	2	3
p-value	0	0.025	0.035
Reject H_0	yes	yes	yes

TABLE 5. *Model analysis*

Model analysis	Results		
Scenario	1	2	3
MLE	-0.13	0.043	-0.02
Forecast error	0	0.4	0.1
Attractor	stable	unstable	stable
Dynamics	fix-point	limit-cycle	limit-cycle
Predictable	yes	short-term	yes
τ^*	1.2	1.2	0.5

3.2. **Scenario 1**

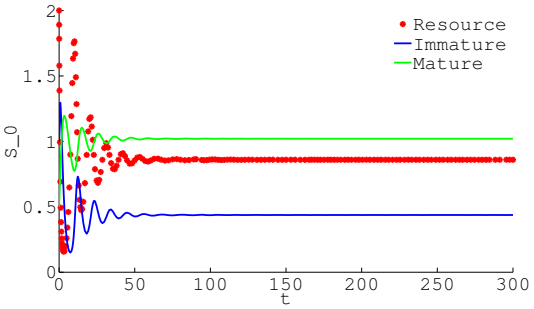

(A) Time Series

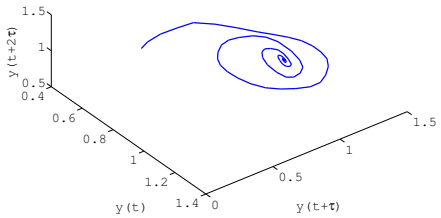

(B) Rec. Phase Space

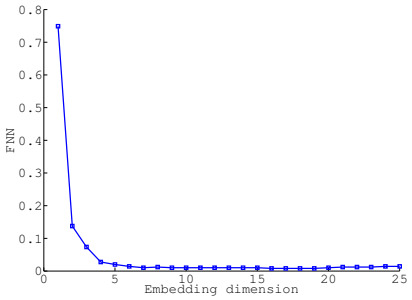

(C) FNN vs. Embedding dimension

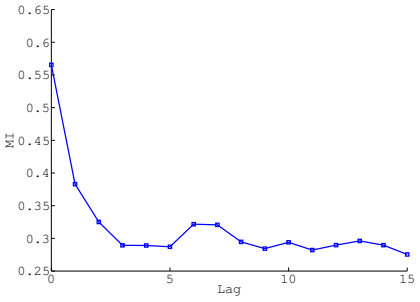

(D) AMI vs. Delay

FIGURE 1. Results of the model analysis–Scenario 1

In Figure 1(A) the trajectory plot presents the time series of the immature, mature and resource for the fixed parameters in Tableau 2 and $\tau_1 = 0.1$. The trajectories converge with oscillatory decay to their equilibrium points $(z^*, x^*, y^*) = (0.860, 0.437, 1.018)$. The mature population follows the dynamics of the immature but

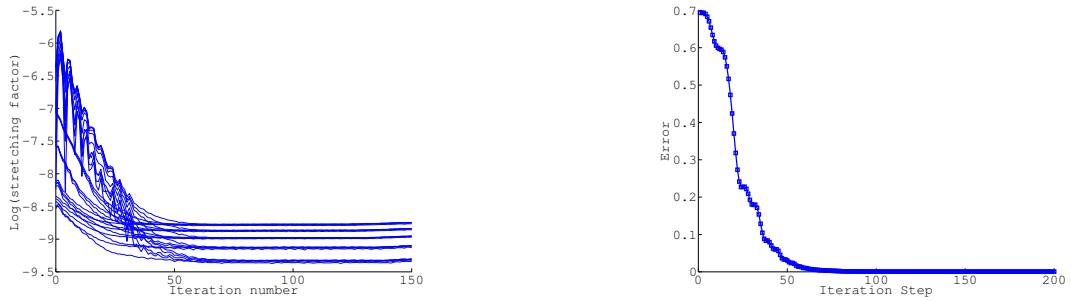

(A) Kantz (B) Forecast error

FIGURE 2. *Result of MLE-algorithm and Forecast–Scenario 1*

with a different amplitude and biomass-density. Figure 1(B) emphasizes the stabilizing tendency of the mature, which results into a fix-point. According to Figure 1(C) the embedding dimension is $D_{E^*} = 4$ and from Figure 1(D), we choose $\tau = 3$.

From Figure 2(A), we compute a negative MLE, $\lambda_1 = -0.13$, at its maximal slope. The system is hence stable.

A negative MLE further indicates that the system is predictable, consistent with the forecast error, which converges to zero with increasing iteration steps, see Figure 2(B). Therefore the forecast time horizon is infinite.

Computational tests have shown that the critical $\tau^* = 1.2$ for the present case.

3.3. **Scenario 2**

Figure 3 shows the dynamics for Scenario 2 and the parameters in Tableau 2 for $\tau_1 = 1.2$. The only difference, compared to Scenario 1, is that the feedback-delay τ_1 is increased in its value. Figure 3(A) shows the model trajectories. The resource, the immature and the mature are oscillating. The constant oscillations are reflected as well in Figure 3(B), where we observe an unstable limit-cycle. From Figure 3(C) the embedding dimension for this case is set to $D_{E^*} = 6$, while we choose $\tau = 15$ according to the AMI plot from Figure 3(D).

From Figure 4(A), we can spot convergence to 1.03, which results in a MLE value of $\lambda_1 = 0.043$. The MLE is approximately zero, though positive. Therefore, we expect the time horizon to be limited. This is consistent with the forecast error in Figure 4(D), where we observe an increase in the error with increasing forecast steps. Hence, the system is not predictable for infinite steps into the future.

Under the same model and resource conditions, as in Scenario 1, we determine $\tau^* = 1.2$.

3.4. **Scenario 3**

Figure 5(A) shows trajectories with decaying oscillations. The time series converge to their theoretical equilibrium $(z^*, x^*, y^*) = (0.863, 0.257, 0.599)$. We choose $\tau_1 = 0.1$ and calculate a negative MLE, $\lambda_1 = -0.02$ from Figure 6(A). According to Figure 5(C) and (D), $D_{E^*} = 4$ and $\tau = 5$.

In Figure 5(B), we observe contracting orbits, which end up in a stable limit cycle, since $\lambda_1 \approx 0$.

Given that MLE < 0 the system is predictable with an infinite future time horizon. The forecast plot in Figure 6(B) matches this result, as the error converges to 0.1 with increasing iteration steps.

Under changed parameter conditions in $\boldsymbol{\theta}$, but otherwise, under equal conditions as in Scenario 1, we calculate $\tau^* = 0.5$.

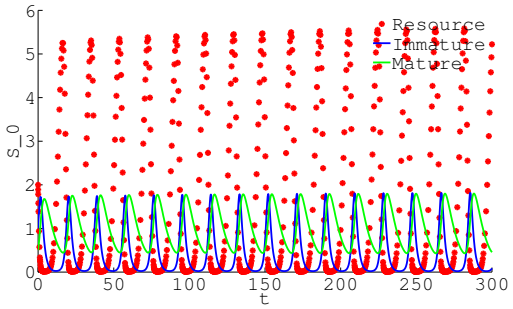

(A) Time Series

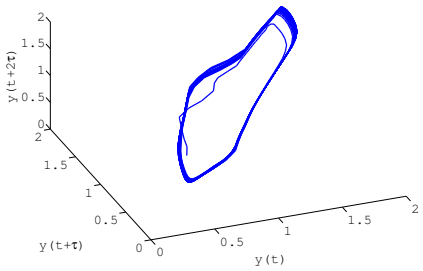

(B) Rec. Phase Space

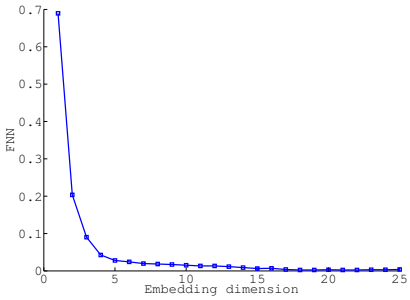

(C) FNN vs. Embedding dimension

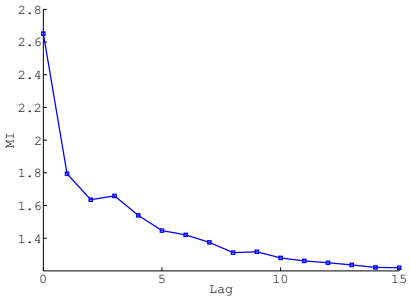

(D) AMI vs. Delay

FIGURE 3. Results of the model analysis–Scenario 2

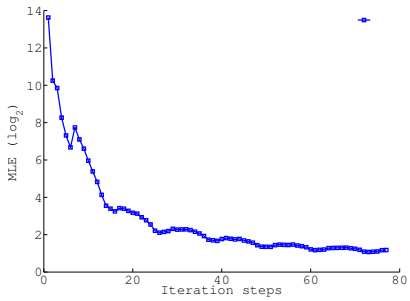

(A) Wolf

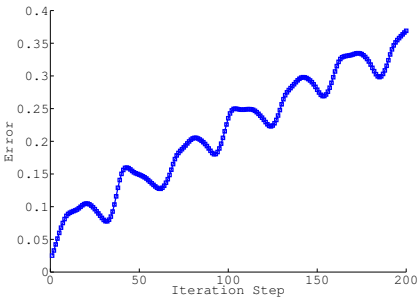

(B) Forecast error

FIGURE 4. *Result of MLE-algorithm and Forecast–Scenario 2*

4. SUMMARY AND DISCUSSION

We start this section with a discussion about the role of the critical delay value, τ^*, and the resource-parameters, $\boldsymbol{\theta}$, for the system dynamics.

From Scenario 2, for $\tau_1 = 1.2$ a limit cycle occurs. From further tests, we observed that for $\tau_1 > 1.2$ the dynamics became chaotic, while we find stable dynamics for $\tau_1 < \tau^*$. For delay values similar to the critical delay, τ^*, limit cycles occur.

Tests from the ODE-systems, i.e. Scenario 1 and 3, showed that for $a = b$, $\tau^* = 1.2$, while for $b > a$, $\tau^* = 0.5$. As Scenario 1 and 3, only differ in the resource-parameters, we observe from these result that a

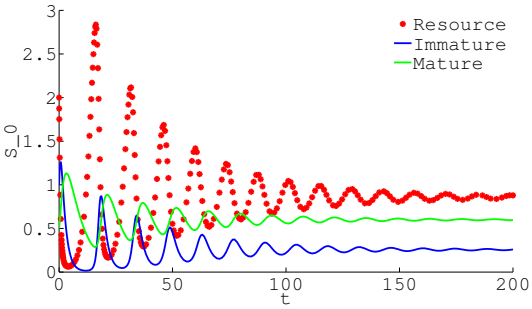

(A) Time Series

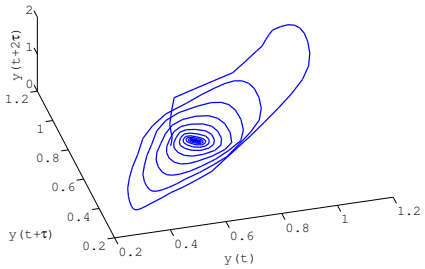

(B) Rec. Phase Space

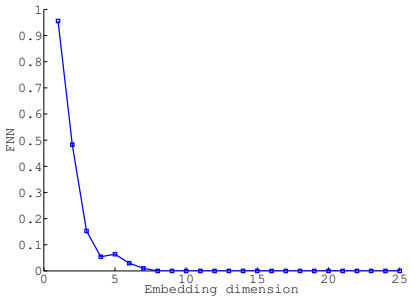

(C) FNN vs. Embedding dimension

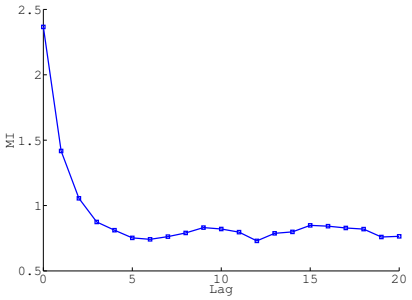

(D) AMI vs. Delay

FIGURE 5. Results of model analysis–Scenario 3

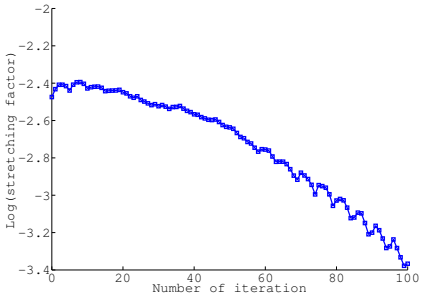

(A) Rosenstein

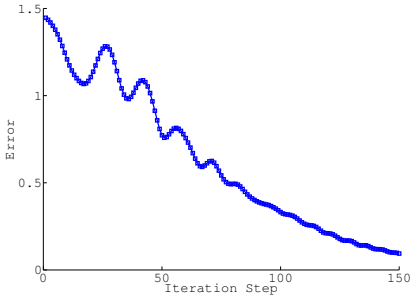

(B) Forecast error

FIGURE 6. *Result of MLE-algorithm and Forecast–Scenario 3*

change in the relation between a and b lead to different critical values of τ^*. For $\tau_1 < \tau^*$, the system results in a stable attractor, while the case for $\tau_1 \geq \tau^*$ leads to an unstable attractor. Comparing this results with Scenario 2, where $\tau_1 = \tau^*$ for $a = b$, we can conclude, that τ^* is fixed, for a constant system S_0, given fixed model parameters, resource-function and -parameters.

Hence, the critical delay value τ^* depends only on the system and its parameters. A change in the resource leads therefore to a change in τ^*. A small τ^*-value, i.e. $\tau^* < 1$, means that the system transits relatively fast into an unstable position, or even into chaos, while a system with a large τ^*-value, i.e. $\tau^* \geq 1$, transits relatively slow. Tableau 6 shows the relationship between the Holling-II function parameters, $\boldsymbol{\theta}$, and the critical delay, τ^*.

TABLE 6. *Resource-function–τ^*-relation*

Resource-function **	$\tau^* \in \mathbb{R}_+$**-value**
slow ($b > a$)	$\tau^* < 1$, (relatively fast transition into chaos)
fast ($a = b$)	$\tau^* \geq 1$, (relatively slow transition into chaos)

(**) The fact that the resource-growth function in the numerical experiments was converging, made the analysis and the interpretation easy. For a system with non-converging resource-growth function, for example, a quadratic resource-growth function, we might draw different conclusions and observe different dynamics.

Assuming, a fixed $\tau_1 \geq 0$ lag in a DDE-system, we can classify two situations due to the relation of τ_1 to τ^* due to our observations:

- For $\tau_1 < \tau^*$, we observe a stable attractor. The system is predictable
- For $\tau_1 \geq \tau^*$, we observe unstable attractors. The systems are not-predictable in the long-term. However, for $\tau_1 = \tau^*$ the system is short-term predictable.

The classification shows that the predictability of the DDE-system depends strongly on the delay-value, as well as the resource-function, which influences τ^* (see Tableau 6), under otherwise constant conditions for system S_0 with fixed parameters from Tableau 2.

The next paragraph summarizes the numerical observations of each scenario.

Scenario 1 represents a case, where $\tau_1 = \tau_2 = 0$. The absence of *delay-interruptions* yielded a negative MLE, which leads to contracting trajectories towards the fix-point attractor. As $\tau^* > 0$, this observation is consistent with the conclusions of the Discussion. The constant biomass flow from the resource into the population-stages allows the mature to develop stable dynamics.

For Scenario 2, the dynamics underwent a limit cycle at $\tau_1 = \tau^* = 1.2$ under the resource-parameter condition of $a = b$. We observed constant oscillation in the immature and mature time series. MLE ≈ 0 indicates that the ellipsoidal axes p_i follow no particular trend. The system orbits evolve therefore to a limit cycle attractor.

The ODE-setting in Scenario 3 leads to contracting system orbits, similar to Scenario 1. This is because there is an uninterrupted stream of resource. We can in addition observe an effect of the resource-growth function on the dynamics compared to Scenario 1. Here the slower convergence of the resource-growth function, as $b > a$, leads to a faster evolution of the matured stage, as we observe a rather small critical delay value $\tau^* = 0.5$. In contrast to Scenario 1, where the dynamic was a fixed point attractor with $\tau^* = 1.2$, the dynamic in Scenario 3 represents a stable limit cycle.

5. CONCLUSION

The analysis has shown that only systems with a small delay-value, i.e. $\tau_1 < \tau^*$, are stable and predictable, see also [42, 43]. The authors of [44] state that DDE-models are chaotic, and representative of e.g. the Ruelle-Takens-Newhouse (RTN) scenario, see [45–47]. The RTN scenario states that a system transits into chaos after three bifurcations, i.e. fixed point–limit cycles–two-tori–three-tori–chaos. We observed for $\tau_1 \approx 0$ that the resource-growth function determines, if the system converges to a fix-point, if $a = b$ or to a limit cycle, if $b > a$, for fixed τ_1. Our results show that for $\tau_1 > \tau^*$ the dynamics became chaotic. These steps are similar to the RTN scenario, see [44]. However, we missed the change into a torus attractor and chaos for fixed τ_1, as our emphasis is not on the dynamic associated with gradual changes of parameter value b, or on bifurcations.

Moreover, the discussion shows that changes in the resource-growth parameters affect the system dynamics, dependent on the system delays. As the critical delay value τ^*, at which the system switches over into chaos can be very small, a discussion of the prediction of a delay-system only makes sense when τ^* is known and the system delay is less then the critical value τ^*.

In [29], we found a similar result except that we considered a two-dimensional transition to instability at the equilibrium points. This manuscript extends the results in [29], by showing that resource-parameters and delays

affect the system predictability. The predictability horizon of the mature population is linked to the transition into chaos, with chaos indicating unpredictability. It has been shown that the resource-growth parameter have influence on the value of τ^*. However, as τ_1 is fixed, a change in the τ^*-value can easily lead to a change of the attractor set as τ^* could become smaller or larger than τ_1. Thus, the resource function influences also the dynamics and stability of the system.

The analysis presented in this manuscript show that each ODE-based model on population dynamics will fail to describe and predict the correct dynamics of the system, if delays are neglected.

References

[1] Whitcher, Brandon and Guttorp, Peter and Percival, Donald B. Wavelet analysis of covariance with application to atmospheric time series. *Journal of Geophysical Research: Atmospheres (1984–2012). Wiley Online Library*, 2000, vol. 105, p. 14941–14962.

[2] Porges, Stephen W and Bohrer, Robert E and Cheung, Michael N and Drasgow, Fritz and McCabe, Philip M and Keren, Gideon. New time-series statistic for detecting rhythmic co-occurrence in the frequency domain: the weighted coherence and its application to psychophysiological research. *Psychological bulletin. American Psychological Association*, 1980, vol. 88, no 3, p. 580.

[3] Hamilton, James D. A new approach to the economic analysis of nonstationary time series and the business cycle. *Econometrica: Journal of the Econometric Society. JSTOR*, 1989, p. 357–384.

[4] Tay, Francis EH and Cao, Lijuan. Application of support vector machines in financial time series forecasting. *Omega. Elsevier*, 2001, vol. 29, no 4, p. 309–317.

[5] Robinson, Enders A. Predictive decomposition of time series with application to seismic exploration. *Journal of Geophysics. Society of Exploration Geophysicists*, 1957, vol. 32, no 3, p. 418–484.

[6] Becks, Lutz and Hilker, Frank M and Malchow, Horst and Jürgens, Klaus and Arndt, Hartmut. Experimental demonstration of chaos in a microbial food web. *Nature. Nature Publishing Group*, 2005, vol. 435, no 7046, p. 1226–1229.

[7] Hurvich, Clifford M and Tsai, Chih-Ling. Regression and time series model selection in small samples. *Biometrika. Biometrika Trust*, 1989, vol. 76, no 2, p. 297–307.

[8] Sugihara, George. Nonlinear forecasting for the classification of natural time series. *Philosophical Transactions of the Royal Society of London A: Mathematical, Physical and Engineering Sciences. The Royal Society*, 1994, vol. 348, no 1688, p. 477–495.

[9] Rosenstein, Michael T and Collins, James J and De Luca, Carlo J. A practical method for calculating largest Lyapunov exponents from small data sets. *Physica D: Nonlinear Phenomena. Elsevier*, 1993, vol. 65, no 1, p. 117–134.

[10] Abarbanel, Henry DI and Rulkov, Nikolai F and Sushchik, Mikhail M. Generalized synchronization of chaos: The auxiliary system approach. *Physical Review. APS*, 1996, vol. 53, no 5, p. 4528.

[11] Gottlieb, Sigal and Shu, Chi-Wang and Tadmor, Eitan. Strong stability-preserving high-order time discretization methods. *SIAM review. SIAM*, 2001, vol. 43, no 1, p. 89–112.

[12] Horton, W and Weigel, RS and Sprott, J Clint. Chaos and the limits of predictability for the solar-wind-driven magnetosphere–ionosphere system. *Physics of Plasmas (1994-present). AIP Publishing*, 2001, vol. 8, no 6, p. 2946–2952.

[13] Ivancevic, Vladimir G and Ivancevic, Tijana T. *High-dimensional chaotic and attractor systems: a comprehensive introduction. Springer Science & Business Media*, 2007, vol. 32.

[14] Yang, Xiao-song and Yang, SS and Duan, CK. Intertwined basins of attraction in systems of ODE. *Chaos, Solitons & Fractals. Elsevier*, 1999, vol. 10, no 9, p. 1453–1456.

[15] Kuang, Yang. *Delay differential equations: with applications in population dynamics. Academic Press*, 1993, vol. 191.

[16] Roussel, M. *Delay-differential equations. Working Paper*, 2005. Available in: http://people. uleth. ca/ roussel/nld/delay. pdf Figura 1: Exemplo 1 Figura 3: Exemplo 3.

[17] Gencay, Ramazan and Dechert, W Davis. An algorithm for the n Lyapunov exponents of an n-dimensional unknown dynamical system. *Physica D: Nonlinear Phenomena. Elsevier*, 1992, vol. 59, no 1, p. 142–157.

[18] Müller, Peter C. Calculation of Lyapunov exponents for dynamic systems with discontinuities. *Chaos, Solitons & Fractals. Elsevier*, 1995, vol. 5, no 9, p. 1671–1681.

[19] Wolf, Alan and Swift, Jack B and Swinney, Harry L and Vastano, John A. Determining Lyapunov exponents from a time series. *Physica D: Nonlinear Phenomena. Elsevier*, 1985, vol. 16, no 3, p. 285–317.

[20] Chen, Wei-Ching. Dynamics and control of a financial system with time-delayed feedbacks. *Chaos, Solitons & Fractals. Elsevier*, 2008, vol. 37, no 4, p. 1198–1207.

[21] Farmer, J Doyne. Chaotic attractors of an infinite-dimensional dynamical system. *Physica D: Nonlinear Phenomena. Elsevier*, 1982, vol. 4, no 3, p. 366–393.

[22] Bryant, Paul and Brown, Reggie and Abarbanel, Henry DI. Lyapunov exponents from observed time series. *Physical Review Letters. APS*, 1990, vol. 65, no 13, p. 1523.

[23] Farmer, J Doyne and Sidorowich, John J. Predicting chaotic time series. *Physical review letters. APS*, 1987, vol. 59, no 8, p. 845.

[24] Hegger, Rainer and Kantz, Holger and Schreiber, Thomas. Practical implementation of nonlinear time series methods: The TISEAN package. *Chaos: An Interdisciplinary Journal of Nonlinear Science. AIP Publishing*, 1999, vol. 9, no 2, p. 413–435.
[25] Penny, William, D. *Signal Processing Course. Institute of Neurology, University College London, Lecture Notes, April*, 1999-2000, http://www.fil.ion.ucl.ac.uk/ wpenny/course/course.html.
[26] Zhang, Jun and Lam, KC and Yan, WJ and Gao, Hang and Li, Yuan. Time series prediction using Lyapunov exponents in embedding phase space. *Computers & Electrical Engineering. Elsevier*, 2004, vol. 30, no 1, p. 1–15.
[27] Taylor, Robert LV. *Attractors: Nonstrange to Chaotic*. 2005.
[28] Valenza, Gaetano and Allegrini, Paolo and Lanatà, Antonio and Scilingo, Enzo Pasquale. Dominant Lyapunov exponent and approximate entropy in heart rate variability during emotional visual elicitation. *Frontiers in neuroengineering. Frontiers Media SA*, 2012, vol. 5.
[29] Frank, Anna S. J., The Effect of Resource Dynamics on Marine Population Trajectories and Stability. *Technical Report. Department of Informatics, University of Bergen, Bergen, Norway*, 2016, no 412.
[30] Berg, Arthur and McMurry, Timothy and Politis, Dimitris N. Testing time series linearity: traditional and bootstrap methods. *Handbook of Statistics: Time Series Analysis: Methods and Applications. Elsevier*, 2012, vol. 30, p. 27.
[31] Vu, Ky M. *Optimal discrete control theory: The rational function structure model. AuLac Technologies Inc.*, 2007.
[32] Kugiumtzis, D. Surrogate data test on time series. *Modelling and Forecasting Financial Data. Springer*, 2002, p. 267–282.
[33] Maiwald, Thomas and Mammen, Enno and Nandi, Swagata and Timmer, Jens. Surrogate data–A qualitative and quantitative analysis. *Mathematical Methods in Signal Processing and Digital Image Analysis. Springer*, 2008, p. 41–74.
[34] Barnett, Adrian G and Wolff, Rodney C. A time-domain test for some types of nonlinearity. *Signal Processing, IEEE Transactions on*. IEEE, 2005. Vol. 53, no 1, p. 26–33.
[35] Doane, David P and Seward, Lori E. Measuring skewness: a forgotten statistic. *Journal of Statistics Education. American Statistical Association. 732 North Washington Street, Alexandria, VA 22314*, 2011, vol. 19, no 2, p. 1–18.
[36] Sauer, Tim and Yorke, James A and Casdagli, Martin. Embedology. *Journal of statistical Physics. Springer*, 1991, vol. 65, no 3-4, p. 579–616.
[37] Fraser, Andrew M and Swinney, Harry L. Independent coordinates for strange attractors from mutual information. *Physical review A. APS*, 1986, vol. 33, no 2, p. 1134.
[38] Frede, Valérie and Mazzega, Pierre. Detectability of deterministic non-linear processes in Earth rotation time-seriesâĂŤII. Dynamics. *Geophysical Journal International. Oxford University Press—*, 1999, vol. 137, no 2, p. 565–579.
[39] Petchey, Owen L and Pontarp, Mikael and Massie, Thomas M and Kéfi, Sonia and Ozgul, Arpat and Weilenmann, Maja and Palamara, Gian Marco and Altermatt, Florian and Matthews, Blake and Levine, Jonathan M and others. The Ecological Forecast Horizon, and examples of its uses and determinants. *Ecology letters. Wiley Online Library*, 2015.
[40] Kantz, Holger and Schreiber, Thomas. *Nonlinear time series analysis. Cambridge university press*, 2004, vol. 7.
[41] Takens, Floris. *Detecting strange attractors in turbulence*. Springer, 1981.
[42] Luo, Jing-Jia and Masson, Sebastien and Behera, Swadhin and Shingu, Satoru and Yamagata, Toshio. Seasonal climate predictability in a coupled OAGCM using a different approach for ensemble forecasts. *Journal of climate*, 2005, vol. 18, no 21, p. 4474–4497.
[43] McMillan, David G. Nonlinear predictability of stock market returns: Evidence from nonparametric and threshold models. *International Review of Economics & Finance. Elsevier*, 2001, vol. 10, no 4, p. 353–368.
[44] Safonov, LA and Tomer, E and Strygin, VV and Ashkenazy, Y and Havlin, S. Delay-induced chaos with multifractal attractor in a traffic flow model. *EPL (Europhysics Letters). IOP Publishing*, 2002, vol. 57, no 2, p. 151.
[45] Eckmann, J-P. Roads to turbulence in dissipative dynamical systems. *Reviews of Modern Physics. APS*, 1981, vol. 53, no 4, p. 643.
[46] Guzmán, AM and Amon, CH. Transition to chaos in converging–diverging channel flows: Ruelle–Takens–Newhouse scenario. *Physics of Fluids (1994-present). AIP Publishing*, 1994, vol. 6, no 6.
[47] Zeytounian, Radyadour Kh. *Theory and applications of viscous fluid flows*. Springer Science & Business Media, 2013.
[48] Sibly, Richard M and Hone, Jim. Population growth rate and its determinants: an overview. *Philosophical Transactions of the Royal Society of London B: Biological Sciences. The Royal Society*, 2002, vol. 357, no 1425, p. 1153–1170.
[49] Turchin, Peter and Batzli, George O. Availability of food and the population dynamics of arvicoline rodents. *Ecology. Eco Soc America*, 2001, vol. 82, no 6, p. 1521–1534.
[50] Rinke, Karsten and Vijverberg, Jacobus. A model approach to evaluate the effect of temperature and food concentration on individual life-history and population dynamics of Daphnia. *Ecological Modelling. Elsevier*, 2005, vol. 186, no 3, p. 326–344.
[51] Previtali, M Andrea and Lima, Mauricio and Meserve, Peter L and Kelt, Douglas A and Gutiérrez, Julio R. Population dynamics of two sympatric rodents in a variable environment: rainfall, resource availability, and predation. *Ecology. Eco Soc America*, 2009, vol. 90, no 7, p. 1996–2006.
[52] Bieber, Claudia and Ruf, Thomas. Population dynamics in wild boar Sus scrofa: ecology, elasticity of growth rate and implications for the management of pulsed resource consumers. *Journal of Applied Ecology. Wiley Online Library*, 2005, vol. 42, no 6, p. 1203–1213.
[53] Wolkowicz, Gail SK; Xia, Huaxing; Ruan, Shigui. Competition in the chemostat: a distributed delay model and its global asymptotic behavior. *SIAM Journal on Applied Mathematics*, 1997, vol. 57, no 5, p. 1281–1310.

[54] Freedman, H. I.; So, Joseph W.-H.; Waltman, Paul. Coexistence in a model of competition in the chemostat incorporating discrete delays. *SIAM Journal on Applied Mathematics*, 1989, vol. 49, no 3, p. 859–870.

[55] Ellermeyer, S. F. Competition in the chemostat: global asymptotic behavior of a model with delayed response in growth. *SIAM Journal on Applied Mathematics*, 1994, vol. 54, no 2, p. 456–465.

[56] Ruan, Shigui; Wolkowicz, Gail SK. Bifurcation analysis of a chemostat model with a distributed delay. *Journal of mathematical analysis and applications*, 1996, vol. 204, no 3, p. 786–812.

[57] Smith, Hal L.; Waltman, Paul. The theory of the chemostat: dynamics of microbial competition. *Cambridge university press*, 1995.

[58] Meng, Xinzhu; Li, Zhenqing; Nieto, Juan J. Dynamic analysis of MichaelisâĂŞMenten chemostat-type competition models with time delay and pulse in a polluted environment. *Journal of Mathematical Chemistry*, 2010, vol. 47, no 1, p. 123.